The Normalized Causal-Past Four-Volume of FLRW Spacetimes as a Diagnostic of the Cosmic Expansion History

Rafael Maya
Independent Researcher, San Diego, California, USA

August 2026

Abstract

The invariant four-volume of an event's causal past is a well-defined geometric functional of a Friedmann–Lemaître–Robertson–Walker expansion history. We study its normalized form, $\mathcal{C}(T) = V_4(T)/V_4(T_0)$, and the family of *causal-fraction ages* T_f defined by $\mathcal{C}(T_f) = f$. We give a closed observable form written entirely in $H(z)$, the exact self-similar limit $T_f \to T_0 f^{1/4}$, and an $O(N)$ moment decomposition enabling per-sample evaluation on posterior chains. Two structural results follow. The dimensionful statistic is almost completely degenerate with the cosmic age (posterior-scaled gradient alignment $\cos\theta = 0.9991$ in flat $w_0 w_a$CDM), whereas the dimensionless ratio $\rho_f \equiv T_f/T_0$ is *exactly* independent of the overall expansion scale. Its sensitivity kernel $K_f(z) = \delta\rho_f/\delta w(z)$ possesses a single sign-change node migrating with f, and at $f_* = 0.2627$ the kernel's lobes cancel exactly: ρ_{f_*} is simultaneously H_0-free and first-order blind to w_0, a differential sensor of dark energy across $z \simeq 0.40$ that within flat ΛCDM tracks the matter–dark-energy handover, $\Omega_\Lambda(z_{f_*}) = 0.46 \pm 0.03$. Transforming every stored sample of the public DESI DR2 BAO+CMB+supernova $w_0 w_a$CDM chains yields $T_{1/6}$ medians displaced by 40–46 Myr (2.5–2.9 posterior standard deviations) from the Planck ΛCDM value $T_{1/6} = 8.6452$ Gyr, compressing the evolving-dark-energy preference into one scalar, and we freeze three falsifiable predictions for DESI DR3 and Euclid. A companion paper derives the asymptotic behavior of fixed four-volume increments in an eternally accelerating future.

1 Introduction

Cosmological inference is usually organized around local or quasi-local observables: the expansion rate $H(z)$, comoving and luminosity distances, and growth functions. A complementary class of quantities integrates the entire expansion history into a single invariant. The four-volume of the past light cone is the most natural member of this class: it is the total amount of spacetime that can have causally influenced a given event. Park and Woodard derived the invariant volume of the past light cone for FLRW geometries and noted its possible role as a geometrically meaningful time variable [1]. Carfora and Familiari have developed light-cone comparison functionals into a quantitative probe of the observed late-time expansion [2, 3]. In causal-set theory, spacetime volume is the fundamental carrier of metric information ("order plus number equals geometry") [4, 5, 6], and in unimodular formulations of general relativity the accumulated four-volume is the variable conjugate to the cosmological constant [7]. The thermodynamics of cosmological horizons, which controls the late-time behavior of causal volumes, is likewise classical material [8].

This paper does not propose new dynamics. It develops the *normalized* causal-past four-volume,

$$\mathcal{C}(T) \equiv \frac{V_4(T)}{V_4(T_0)}, \qquad 0 \leq \mathcal{C}(T) \leq 1, \tag{1}$$

as a practical diagnostic of the expansion history, where T_0 is the present cosmic age. Three questions are addressed. First, what is the cleanest observable form of the statistic—that is, how does an empirical $H(z)$ determine the *causal-fraction age* T_f at which a fraction f of the present causal four-volume has accumulated? Second, how much cosmological information does T_f carry, and in which parameter directions? Third, how can the statistic be evaluated efficiently enough to transform full posterior chains sample by sample? The fraction f is kept as a free parameter throughout; particular rational values such as $f = 1/6$ are used only as worked illustrations.

The answers are, in brief: (i) the defining condition can be written as a ratio of double integrals of $1/H(z)$ alone, Eqs. (6)–(7); (ii) the dimensionful statistic T_f is almost completely degenerate with the cosmic age t_0 within flat w_0w_aCDM, whereas the dimensionless ratio $\rho_f = T_f/T_0$ is an exactly scale-free probe of the shape of the late-time expansion; and (iii) a moment decomposition reduces the cost of a full clock curve to four cumulative one-dimensional integrals, which makes chain-level transformations routine. Section 9 demonstrates the machinery on the public DESI DR2 flat w_0w_aCDM chains [10].

Concretely, the paper establishes seven results:

1. a closed, model-independent observable form of the causal-fraction age as a pure integral functional of $H(z)$, Eqs. (6)–(7), directly applicable to non-parametric reconstructions;

2. the universal self-similar law $V_4 \propto T^4$ and its boundary corollary $T_f = T_0 f^{1/4}$, an exact analytic benchmark for any implementation;

3. a quantitative degeneracy theorem for the dimensionful statistic—its posterior-scaled gradient is aligned with that of the cosmic age to $\cos\theta = 0.99912$ within flat w_0w_aCDM—together with the exact H_0-independence of the dimensionless ratio ρ_f;

4. the existence of a distinguished fraction $f_* = 0.2627$ at which $\partial\rho_f/\partial w_0$ vanishes, so that ρ_{f_*} is simultaneously blind to the expansion scale (exactly) and to the present dark-energy equation of state (to first order), isolating (Ω_m, w_a);

5. the redshift sensitivity kernel $K_f(z) = \delta\rho_f/\delta w(z)$ of the family, which possesses a single sign-change node migrating with f; the w_0 blindness at f_* is shown to be an exact lobe cancellation of this kernel, so ρ_{f_*} measures the *contrast* of dark-energy behavior below versus above $z \simeq 0.40$ (Section 7);

6. a physical characterization of the blind point: it is exactly H_0-independent and, within flat ΛCDM, tracks the matter–dark-energy handover at $\Omega_\Lambda(z_{f_*}) = 0.46 \pm 0.03$, with quantified second-order w_0 leakage and an honest account of its fiducial dependence;

7. an $O(N)$ moment-decomposition algorithm and its first application to complete public posterior chains, yielding a single-scalar compression of the DESI DR2 evolving-dark-energy preference and a sharp null test for future data releases.

2 Geometry of the causal-past four-volume

For a spatially flat FLRW universe in spherical comoving coordinates,

$$\mathrm{d}s^2 = -c^2\mathrm{d}t^2 + a^2(t)\left(\mathrm{d}r^2 + r^2\mathrm{d}\Omega^2\right), \qquad \mathrm{d}\Omega^2 = \mathrm{d}\theta^2 + \sin^2\theta\,\mathrm{d}\phi^2. \tag{2}$$

A radial null ray satisfies $\mathrm{d}r = c\,\mathrm{d}t/a(t)$. For an endpoint at cosmic time T, define the comoving light-cone radius, physical radius, and physical three-volume of the slice at time $t \le T$,

$$\chi(t,T) \equiv \int_t^T \frac{c\,\mathrm{d}u}{a(u)}, \qquad R(t,T) \equiv a(t)\,\chi(t,T), \qquad V_3(t;T) \equiv \frac{4\pi}{3} R^3(t,T). \tag{3}$$

The causal-past four-volume is the proper-time accumulation of these slices,

$$V_4(T) \equiv c\int_0^T V_3(t;T)\,\mathrm{d}t = \frac{4\pi c}{3}\int_0^T a^3(t)\left[\int_t^T \frac{c\,\mathrm{d}u}{a(u)}\right]^3 \mathrm{d}t. \tag{4}$$

Equation (4) is standard light-cone geometry written explicitly for the quantity used here [1]; a self-contained derivation, including the equivalence of the spherical and Cartesian forms, is given in Appendix A. The normalized functional is Eq. (1), and the causal-fraction age T_f is the unique root of

$$\boxed{\mathcal{C}(T_f) = f, \qquad 0 < f < 1.} \tag{5}$$

Uniqueness follows because $V_4(T)$ is strictly increasing. The family $\{T_f\}$ is a reparametrization of cosmic history by accumulated causal volume rather than by proper time; the map $f \mapsto T_f$ is smooth and monotonic, and any particular f may be used as a scalar compression of the expansion history.

3 Observable form in terms of $H(z)$

The condition (5) can be written without first solving for $a(t)$. With $a = (1+z)^{-1}$ and $\mathrm{d}t = -\mathrm{d}z/[(1+z)H(z)]$, the cosmic age associated with the boundary redshift z_f is

$$T_f = \int_{z_f}^{\infty} \frac{\mathrm{d}z}{(1+z)\,H(z)}, \tag{6}$$

and the fraction condition becomes

$$\boxed{f\int_0^{\infty} \frac{\mathrm{d}z'}{(1+z')^4 H(z')}\left[\int_0^{z'} \frac{\mathrm{d}z''}{H(z'')}\right]^3 = \int_{z_f}^{\infty} \frac{\mathrm{d}z'}{(1+z')^4 H(z')}\left[\int_{z_f}^{z'} \frac{\mathrm{d}z''}{H(z'')}\right]^3.} \tag{7}$$

Equations (6)–(7) are the central formulas of this paper. They contain no reference to a specific parameterization: a non-parametric reconstruction of $H(z)$ from BAO, supernovae, cosmic chronometers, or standard sirens can be inserted directly, making T_f an integral functional of data-level quantities. The derivation is given in Appendix B.

Table 1 | Causal-fraction ages at selected fractions. Flat ΛCDM baseline versus the DESI DR2 flat w_0w_aCDM (Pantheon+) central fit. Ages in Gyr.

f	1/12	2/12	3/12	4/12	6/12	9/12
ΛCDM baseline	7.303	8.645	9.588	10.336	11.522	12.849
w_0w_aCDM central	7.269	8.605	9.548	10.297	11.487	12.822
Difference (Myr)	−33.7	−39.8	−40.1	−38.8	−35.2	−26.9

4 The self-similar limit

During a self-similar epoch $a(t) = A\,t^p$, direct substitution into Eq. (4) and the rescaling $t = xT$ give (Appendix C)

$$V_4(T) = C(p)\,c^4\,T^4, \qquad C(p) = \frac{4\pi}{3(1-p)^3}\int_0^1 x^{3p}\big(1 - x^{1-p}\big)^3 \mathrm{d}x, \tag{8}$$

so the exponent is universal: $V_4 \propto T^4$ for any single power law. Equal volume fractions then obey the scale-free boundary law

$$T_f \simeq T_0\, f^{1/4}. \tag{9}$$

For the baseline age $T_0 = 13.795181$ Gyr, Eq. (9) gives $T_{1/6}^{(t^4)} = 8.814336$ Gyr, whereas the exact calculation of Section 5 gives 8.645194 Gyr. The 169 Myr displacement measures the departure of the observed expansion history from any single self-similar power law, and Eq. (9) provides a useful analytic check on numerical implementations.

5 Baseline evaluation

Unless stated otherwise, numerical examples use flat ΛCDM with $H_0 = 67.36\ \mathrm{km\,s^{-1}\,Mpc^{-1}}$, $\Omega_m = 0.3153$, $\Omega_r = 9.209 \times 10^{-5}$, and $\Omega_\Lambda = 1 - \Omega_m - \Omega_r$, following the Planck-2018 base-ΛCDM analysis [9]. Numerical integration of Eq. (4) on a quadratic scale-factor grid and Brent root solution [25] of Eq. (5) give, for $f = 1/6$,

$$T_{1/6} = 8.645194\ \text{Gyr}, \qquad a_{1/6} = 0.670454, \qquad z_{1/6} = 0.491527, \tag{10}$$

with present age $T_0 = 13.795181$ Gyr. Grid convergence is documented in Appendix D: doubling the grid from 16,001 to 32,001 nodes changes $T_{1/6}$ by 9 years, so the printed decimals describe the deterministic calculation with frozen inputs, not observational precision.

Figure 1 shows the normalized clock together with the self-similar limit; Fig. 2 shows the full family T_f for the baseline and for a representative evolving-dark-energy history, the DESI DR2 (DESI+CMB+Pantheon+) flat w_0w_aCDM central fit $(H_0, \Omega_m, w_0, w_a) = (67.51,\ 0.3114,\ -0.838,\ -0.62)$ [10]. Table 1 lists T_f at selected twelfths for both histories. The evolving-dark-energy history lowers T_f at every fraction, by 34–40 Myr in the range $f \in [1/12, 1/2]$; the difference is a smooth, slowly varying offset over the central fractions, which anticipates the near-degeneracy quantified in Section 6.

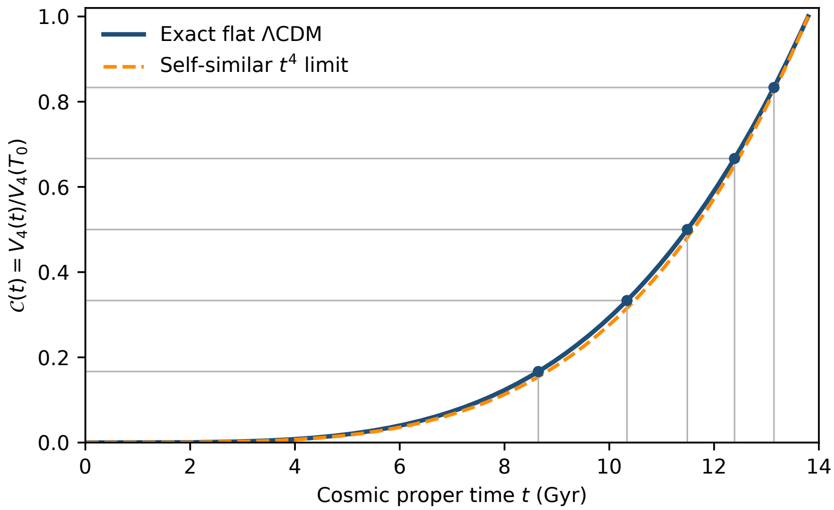

Figure 1 | The normalized causal clock. $\mathcal{C}(t)$ for the Planck-2018 baseline (solid) and the self-similar t^4 limit of Eq. (9) (dashed). Markers show the causal-fraction ages $T_{n/6}$; the guides indicate how each fraction f defines a unique age T_f.

6 Information content: sensitivities and degeneracy structure

A new statistic is only useful if its response directions in parameter space are known. Within flat w_0w_aCDM,

$$H^2(a) = H_0^2\Big[\Omega_r a^{-4} + \Omega_m a^{-3} + (1-\Omega_r-\Omega_m)\,a^{-3(1+w_0+w_a)}e^{-3w_a(1-a)}\Big], \tag{11}$$

with the Chevallier–Polarski–Linder form $w(a) = w_0 + w_a(1-a)$ [11, 12], central finite differences of the exact boundary about the baseline $(H_0, \Omega_m, w_0, w_a) = (67.36, 0.3153, -1, 0)$ give

$$\frac{\partial T_{1/6}}{\partial H_0} = -0.12823\ \frac{\text{Gyr}}{\text{km s}^{-1}\,\text{Mpc}^{-1}}, \qquad \frac{\partial T_{1/6}}{\partial \Omega_m} = -7.1945\ \text{Gyr},$$
$$\frac{\partial T_{1/6}}{\partial w_0} = -1.2863\ \text{Gyr}, \qquad \frac{\partial T_{1/6}}{\partial w_a} = -0.26282\ \text{Gyr}, \tag{12}$$

while the same differentiation applied to the cosmic age gives

$$\frac{\partial t_0}{\partial H_0} = -0.20464\ \frac{\text{Gyr}}{\text{km s}^{-1}\,\text{Mpc}^{-1}}, \qquad \frac{\partial t_0}{\partial \Omega_m} = -12.312\ \text{Gyr},$$
$$\frac{\partial t_0}{\partial w_0} = -2.0254\ \text{Gyr}, \qquad \frac{\partial t_0}{\partial w_a} = -0.45747\ \text{Gyr}. \tag{13}$$

The radiation density is recomputed at each parameter point from $\Omega_r h^2 = 4.18343 \times 10^{-5}$.

6.1 The dimensionful statistic is nearly degenerate with the age

To compare information directions on a common footing, scale each gradient component by a representative marginal posterior width of the DESI DR2 flat w_0w_aCDM combination,

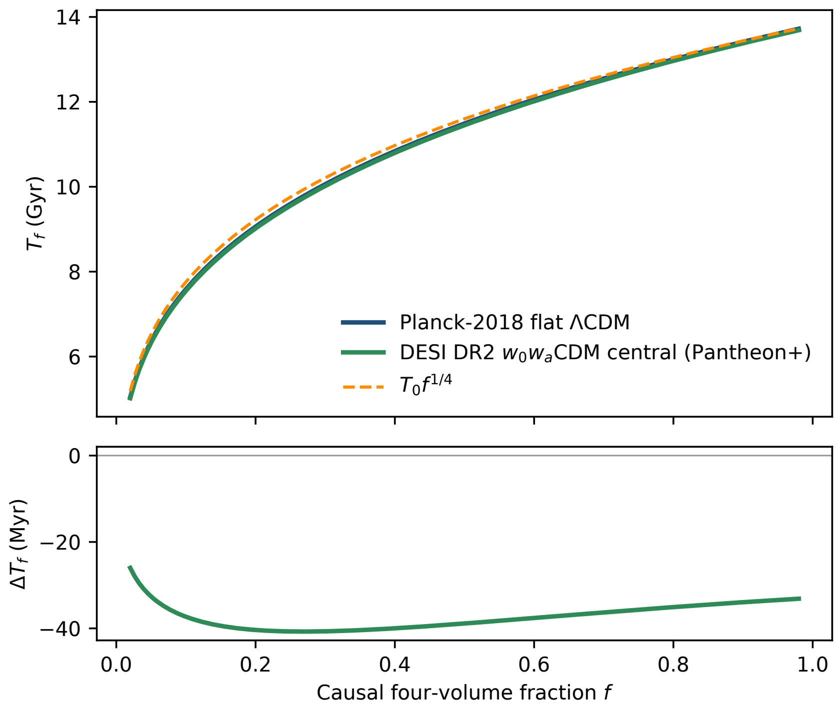

Figure 2 | The causal-fraction age family. Top: T_f for the Planck-2018 baseline, for the DESI DR2 flat w_0w_aCDM central fit combined with Pantheon+, and the quarter-power law $T_0 f^{1/4}$. Bottom: the difference between the two exact histories in Myr.

$(\sigma_{H_0}, \sigma_{\Omega_m}, \sigma_{w_0}, \sigma_{w_a}) = (0.59,\ 0.0057,\ 0.055,\ 0.22)$ [10]. The cosine of the angle between the scaled gradients of $T_{1/6}$ and t_0 is

$$\cos\theta\big(\nabla T_{1/6}, \nabla t_0\big) = 0.99912, \qquad \theta = 2.40^\circ, \qquad \sin^2\theta = 1.8\times 10^{-3}. \tag{14}$$

The dimensionful causal-fraction age therefore carries essentially no direction of information that the ordinary age integral does not already carry: as a posterior statistic within this parameterization, T_f is a smooth reparametrization of t_0 at the 0.2% level of the orthogonal complement. Figure 3 makes this visible: the level curves of $T_{1/6}$ and t_0 in the (Ω_m, H_0) plane are nearly parallel. This is an honest characterization rather than a limitation of the machinery; it locates the statistic within the family of age-like functionals whose incremental constraining power over standard chains is known to be modest in ΛCDM-like models.

6.2 The dimensionless ratio is an exact shape statistic

The situation changes for the dimensionless fraction ratio

$$\boxed{\rho_f \equiv \frac{T_f}{T_0}, \qquad \rho_{1/6} = 0.626682 \text{ (baseline)}.} \tag{15}$$

At fixed dimensionless densities and equation-of-state parameters, every occurrence of H in Eqs. (6)–(7) contributes the same power of H_0 to numerator and denominator, so z_f is H_0-independent and both T_f and T_0 scale as H_0^{-1}: the ratio ρ_f is *exactly* independent of the overall

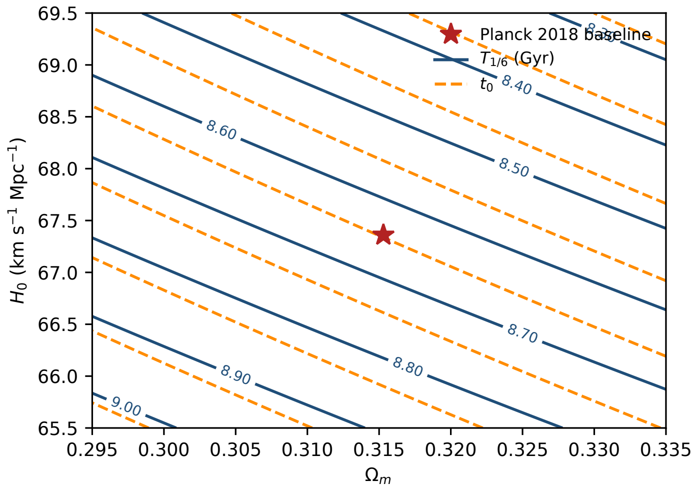

Figure 3 | Degeneracy with the cosmic age. Level curves of $T_{1/6}$ (solid, labeled in Gyr) and of t_0 (dashed) in the (Ω_m, H_0) plane for flat ΛCDM. The two families are nearly parallel, the quantitative statement being Eq. (14).

expansion scale. (The residual numerical derivative $\partial\rho_{1/6}/\partial H_0 = 1.1 \times 10^{-6}$ per $\mathrm{km\,s^{-1}\,Mpc^{-1}}$ arises only through the h-dependence of Ω_r and is negligible.) The remaining sensitivities are

$$\frac{\partial\rho_{1/6}}{\partial\Omega_m} = 0.0378, \qquad \frac{\partial\rho_{1/6}}{\partial w_0} = -0.00124, \qquad \frac{\partial\rho_{1/6}}{\partial w_a} = 0.00173, \tag{16}$$

equivalently $\partial \ln\rho_{1/6}/\partial\theta_i = (0.0603,\ -0.00197,\ 0.00276)$. In posterior-scaled units the ordering is w_a (3.8×10^{-4}), Ω_m (2.2×10^{-4}), w_0 (0.7×10^{-4}): the ratio statistic is dominated by the late-time shape parameters, with the evolution parameter w_a the single largest contributor. Figure 4 extends both sets of sensitivities across the full range of f.

The w_0 response of the ratio statistic, moreover, changes sign across the family: at the baseline cosmology,

$$\left.\frac{\partial\rho_f}{\partial w_0}\right|_{f=f_*} = 0, \qquad \boxed{f_* = 0.2627, \qquad T_{f_*} = 9.720\ \text{Gyr}, \qquad \rho_{f_*} = 0.70460.} \tag{17}$$

At this distinguished fraction the statistic is simultaneously independent of H_0 (exactly) and of w_0 (to first order): ρ_{f_*} is a targeted probe of the matter density and of the dark-energy *evolution* parameter w_a alone. No other single background observable in common use shares this property, which makes ρ_{f_*} a natural consistency variable for separating "w_0-like" from "w_a-like" departures from ΛCDM. Section 7 locates this point physically, derives the mechanism of its blindness, and situates the construction relative to prior nulling techniques. The practical conclusion is a clean division of labor: T_f inherits the full H_0 leverage of an age measurement, while ρ_f deletes the scale exactly and isolates shape information, making the pair (T_0, ρ_f) an equivalent but physically transparent repackaging of the age-like content of a chain.

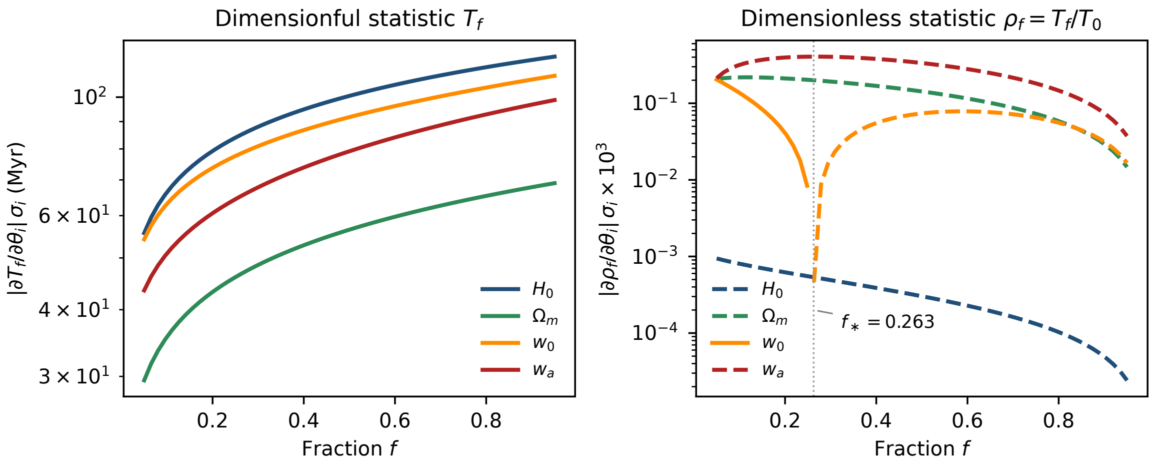

Figure 4 | Posterior-scaled sensitivities across the fraction family. Left: absolute scaled derivatives $|\partial T_f/\partial\theta_i|\,\sigma_i$ in Myr for $\theta_i \in \{H_0, \Omega_m, w_0, w_a\}$. Right: the same for the dimensionless ratio ρ_f; the H_0 curve sits three orders of magnitude below the shape parameters, reflecting the exact cancellation of the expansion scale. Solid segments denote negative derivatives, dashed segments positive ones; the w_0 curve dips to zero at the sign change $f_* = 0.263$ of Eq. (17), where ρ_f becomes first-order blind to w_0.

7 Physical location and mechanism of the w_0-blind fraction

7.1 The sensitivity kernel and its node

The blindness of ρ_{f_*} to w_0 has a transparent mechanism, made visible by the redshift sensitivity kernel of the family. Define the functional derivative of the ratio statistic with respect to a localized change of the dark-energy equation of state,

$$K_f(z) \equiv \left.\frac{\delta\rho_f}{\delta w(z)}\right|_{\Lambda\mathrm{CDM}}, \qquad \frac{\partial\rho_f}{\partial w_0} = \int_0^\infty K_f(z)\,\mathrm{d}z, \tag{18}$$

computed numerically by perturbing $w \to -1 + \Delta w$ in narrow redshift bins and recording the response of ρ_f per unit Δw per unit redshift. Figure 5 (left) shows $K_f(z)$ for $f = 1/6$, f_*, and $1/2$. Every member of the family has the same structure: a negative low-redshift lobe, a positive high-redshift lobe, and a *single* sign-change node that migrates monotonically with the fraction,

$$z_{\mathrm{node}}(1/6) = 0.473, \qquad z_{\mathrm{node}}(f_*) = 0.399, \qquad z_{\mathrm{node}}(1/2) = 0.293. \tag{19}$$

Because a constant shift of w_0 integrates the kernel over all redshift, the w_0 response of ρ_f is the *signed area* of K_f; the special fraction $f_* = 0.2627$ is precisely the member at which the two lobes cancel exactly. The blindness is therefore not an accident of parameterization but an integral null: at f_*, the statistic responds only to redshift dependence of w that breaks the cancellation. Equivalently, ρ_{f_*} is a *differential sensor* of dark energy, comparing its behavior below the node ($z \lesssim 0.40$) against its behavior above it. This is exactly why the evolution parameter w_a, which tilts $w(z)$ across the node, dominates the residual sensitivity of Eq. (16).

The kernel also quantifies how far the first-order statement extends. Sweeping a constant w_0 across the range preferred by current data, the response of ρ_{f_*} is quadratic to excellent approximation,

$$\rho_{f_*}(w_0) - \rho_{f_*}(-1) \simeq 0.0135\,(1 + w_0)^2, \tag{20}$$

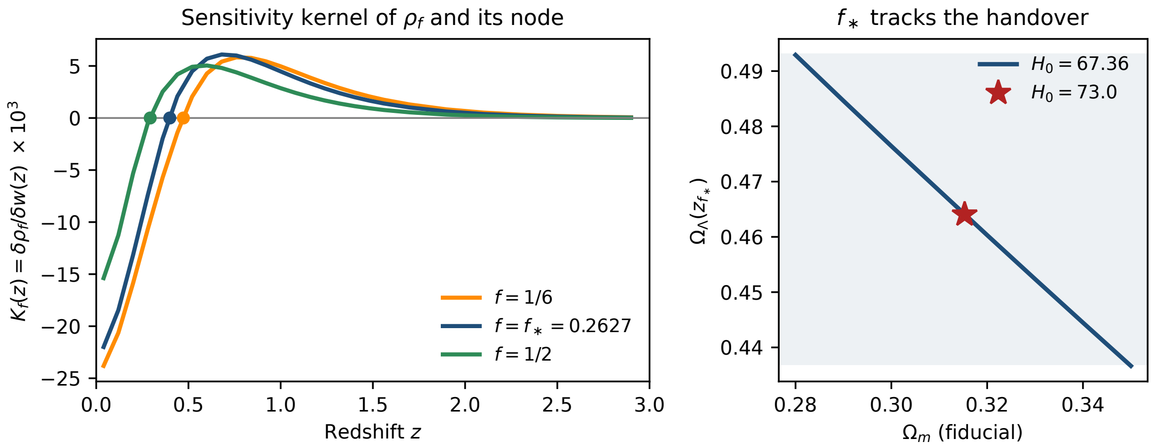

Figure 5 | Kernel, node, and handover tracking. Left: the sensitivity kernel $K_f(z) = \delta\rho_f/\delta w(z)$ for three fractions, computed by localized equation-of-state perturbations about the Planck baseline. Each kernel has a single sign-change node (markers) migrating with f; at f_* the signed area vanishes, which is the mechanism of the w_0 blindness. Right: within flat ΛCDM, the dark-energy fraction at the blind epoch stays inside $\Omega_\Lambda(z_{f_*}) = 0.437$–$0.493$ (shaded) across the plausible matter-density range, and is exactly unchanged by moving H_0 from 67.36 to 73 (star).

with residual linear coefficient 6×10^{-4} attributable to the finite rounding of f_*. The second-order leakage is 2.2×10^{-4} at $w_0 = -0.85$ and 2.0×10^{-3} at $w_0 = -0.6$: for excursions $|1 + w_0| \lesssim 0.15$ it remains below the width of the ΛCDM fingerprint band of Section 10 ($\pm 2.7 \times 10^{-4}$), while for the larger departures entertained by some current fits it becomes appreciable. All blindness statements in this paper are therefore to be read as first-order and fiducial-conditional, with Eq. (20) supplying the quantitative boundary of their validity.

7.2 The blind point tracks the matter–dark-energy handover

Where does f_* fall in cosmic history? At the baseline cosmology the blind epoch is $T_{f_*} = 9.720$ Gyr, i.e. redshift $z_{f_*} = 0.358$, where dark energy supplies a fraction $\Omega_\Lambda(z_{f_*}) = 0.464$ of the total density. Two robustness properties elevate this from a numerical curiosity to a physical characterization. First, because the normalized clock is independent of the expansion scale, the triple $(f_*, z_{f_*}, \Omega_\Lambda(z_{f_*}))$ is *exactly* H_0-independent: recomputing at $H_0 = 73\ \mathrm{km\,s^{-1}\,Mpc^{-1}}$ leaves all three unchanged to four decimals (0.2627, 0.3585, 0.4641), only the dimensionful T_{f_*} rescaling to 8.969 Gyr. Second, sweeping the matter density across $\Omega_m = 0.28$–0.35 moves $\Omega_\Lambda(z_{f_*})$ only within 0.437–0.493 (Fig. 5, right). Within flat ΛCDM, therefore,

$$\boxed{\Omega_\Lambda(z_{f_*}) = 0.46 \pm 0.03} \tag{21}$$

across the observationally allowed range: *the w_0-blind fraction is the causal-volume marker of the matter-to-dark-energy handover*, the epoch at which dark energy is about to take over the cosmic budget. This is also the intuitive content of the kernel mechanism: the node must sit where dark energy is dynamically significant but not yet dominant, since only there can the early and late lobes balance.

Honesty requires the converse statement. Under non-ΛCDM fiducials the blind point migrates substantially: $f_* = 0.123$ at $(w_0, w_a) = (-0.9, 0)$ and $f_* = 0.430$ at the DESI DR2 CPL central fit $(-0.838, -0.62)$. The blindness is anchored to the ΛCDM null hypothesis; the migration of the node under alternative fiducials is not a defect but part of the diagnostic, since prediction P2 of Section 10 is formulated at the ΛCDM-anchored point.

7.3 No coincidence with a named epoch

For completeness we record that no named event of cosmic history coincides with the blind epoch. At the baseline cosmology, matter–dark-energy density equality ($\rho_m = \rho_\Lambda$) occurs at $z = 0.295$ (age 10.303 Gyr) and the onset of acceleration ($q = 0$) at $z = 0.631$ (age 7.696 Gyr); the blind epoch $z_{f_*} = 0.358$ (age 9.720 Gyr) lies between them and coincides with neither, and $\Omega_\Lambda(z_{f_*}) = 0.464$ is not one-half. The correct statement is the window characterization of Eq. (21), not a coincidence. Two observationally useful facts do attach to the location: $z_{f_*} = 0.358$ falls between the effective redshifts of the two best-sampled low-redshift DESI tracers (BGS at $z_{\rm eff} = 0.295$ and LRG1 at $z_{\rm eff} = 0.510$), and the node redshift $z_{\rm node} \simeq 0.40$ lies numerically inside the range of pivot redshifts (~ 0.25–0.5) reported for current data combinations—a corroboration expected on physical grounds, though the two objects are distinct, as discussed next.

7.4 Relation to prior nulling constructions

Four established techniques are adjacent to this construction, and the distinctions matter. *(i) The pivot redshift* [19, 20] is the redshift at which a given dataset's uncertainty on w is minimized and w_p decorrelates from w_a; it is a property of an experiment's covariance and moves with the survey. The node of Eq. (19) is instead a property of a fixed geometric observable at a fiducial cosmology, independent of any dataset or noise model; the numerical proximity of $z_{\rm node} \simeq 0.40$ to typical pivots is expected—both are anchored to the epoch where dark energy begins to matter—but the objects are constructed differently. *(ii) Linear-response kernels of distance observables* [21, 22] establish that distances and ages respond to $w(z)$ through *single-signed* weighting kernels; in particular the comoving-distance kernel of Ref. [22] is negative-definite and low-pass in character. The kernel of the normalized four-volume ratio is, to our knowledge, the first *sign-changing* sensitivity kernel of a scalar background statistic exhibited in this context, and the sign change is what makes an integral null—and hence a w_0-blind member of the family—possible at all. *(iii) Blind redshift spots* [23] are pointwise zeros of $\partial O(z)/\partial p$ for redshift-resolved observables; the present null is an integral cancellation within a single scalar, not a pointwise zero. *(iv) Nulling and decorrelation techniques* in weak lensing and $w(z)$ principal-component analysis [24] engineer data weights to remove unwanted modes for a given survey; the construction here requires no data weights, because the null is supplied by the geometry of the observable itself. The narrow novelty claim of this paper is accordingly: a one-parameter family of integral background observables whose sign-changing sensitivity kernel contains a member with an exact integral null of the present-day equation of state.

8 Fast evaluation: moment decomposition

Direct evaluation of Eq. (4) is expensive on posterior chains because the integral is nested. Let $\eta(T) = \int_0^T \mathrm{d}t/a(t)$ denote conformal time. Then $V_4(T) \propto \int_0^T a^3(t)\,[\eta(T) - \eta(t)]^3\,\mathrm{d}t$, and

Table 2 | Posterior of the causal-fraction age under DESI DR2. Weighted medians and central 68% intervals of $T_{1/6}$ from the flat w_0w_aCDM chains, the displacement $\Delta \equiv T_{1/6} - T^{\Lambda}_{1/6}$ from the Planck ΛCDM baseline value $T^{\Lambda}_{1/6} = 8.6452$ Gyr, and the recomputed central-fit values as a cross-check.

SN likelihood	Rows	$T_{1/6}$ (Gyr)	Δ (Myr)	Central-fit $T_{1/6}$ (Gyr)
Pantheon+	100,918	$8.6043^{+0.0161}_{-0.0158}$	$-40.9^{+16.1}_{-15.8}$	8.6054
Union3	108,724	$8.5993^{+0.0163}_{-0.0160}$	$-45.9^{+16.3}_{-16.0}$	8.5990
DES-SN5YR	61,168	$8.6006^{+0.0157}_{-0.0157}$	$-44.6^{+15.7}_{-15.7}$	8.5998

expanding the cube defines four cumulative moments

$$M_k(T) = \int_0^T a^3(t)\, \eta^k(t)\, \mathrm{d}t, \qquad k = 0, 1, 2, 3, \tag{22}$$

in terms of which

$$\boxed{V_4(T) \propto \eta_T^3 M_0(T) - 3\eta_T^2 M_1(T) + 3\eta_T M_2(T) - M_3(T), \qquad \eta_T \equiv \eta(T).} \tag{23}$$

A single sweep over a scale-factor grid therefore yields the complete clock curve $\mathcal{C}(a)$, from which any set of fractions $\{f\}$ is read off by interpolation: the cost per posterior sample is that of four cumulative one-dimensional integrals, $O(N)$ in the grid size. Against an independent nested-quadrature implementation with $N = 8001$ nodes, the moment method with $N = 2049$ reproduces $T_{1/6}$ to better than 8×10^{-6} Gyr across dispersed chain rows, three orders of magnitude below the posterior widths encountered in Section 9. Algorithmic details and grid-convergence tables are collected in Appendix D.

9 Worked example: transformation of the DESI DR2 posterior chains

As a demonstration on real data we transform the public DESI DR2 flat w_0w_aCDM Cobaya chains, combining all DR2 BAO measurements with the baseline CMB likelihood and, separately, the Pantheon+ [13], Union3 [14], and DES-SN5YR [15] supernova compilations [10]. For every stored row $\theta_i = (H_0, \Omega_m, w_0, w_a, \dots)_i$ the statistic is evaluated once,

$$\theta_i \;\longmapsto\; T_{1/6,i}, \tag{24}$$

with the released multiplicity weights q_i retained and no thinning, resampling, or Gaussian approximation. The radiation fraction is recomputed per sample from $\Omega_r h^2 = 4.18343 \times 10^{-5}$; the moment decomposition of Section 8 is used with $N = 2049$ nodes. Chain-handling details are in Appendix E. The choice $f = 1/6$ is illustrative; because the map $f \mapsto T_f$ is smooth (Fig. 2), nearby fractions carry the same information.

Table 2 gives the result. Two points deserve emphasis. First, the posterior of a deeply nested, nonlinear functional of $H(z)$ is obtained here at chain level, with the full parameter covariance and non-Gaussian structure propagated exactly; comparison of the weighted medians with the values recomputed at the published marginalized central fits (final column) shows agreement at the few-Myr level, confirming that in this instance the central-value substitution is a good approximation—something that could not have been asserted without the full transform. Second, the statistic provides a one-number expression of the current evolving-dark-energy preference: relative to the Planck ΛCDM baseline value 8.6452 Gyr, all three combinations displace $T_{1/6}$ downward by 41–46 Myr, i.e. by ≈ 2.5–2.9 posterior standard deviations of the statistic itself. This compression mirrors, in a single scalar, the 2.8–4.2σ preference for $w_0 > -1$, $w_a < 0$ reported by the DESI collaboration for these data combinations [10].

Two caveats bound the interpretation. The significance of the dynamical-dark-energy preference is itself under active discussion: the relative weight of the three supernova compilations has been questioned [16], and recalibration of the DES sample has been reported to lower the joint preference [17, 18]. The transform presented here is agnostic on that debate; it demonstrates how any resolution of it propagates into the causal statistic. And, per Section 6, the displacement in $T_{1/6}$ is not *independent* evidence—it is the age-like projection of the same chains, offered as a compact, geometrically interpretable summary rather than as a new constraint.

10 Discussion

The normalized causal-past four-volume supplies a one-parameter family of scalar functionals T_f of the expansion history with four useful properties: a closed observable form in $H(z)$ alone, Eqs. (6)–(7); an exact self-similar benchmark $T_f = T_0 f^{1/4}$; an $O(N)$ evaluation scheme suitable for full posterior chains; and a clean information-theoretic characterization—the dimensionful statistic is a near-exact reparametrization of the cosmic age (alignment 0.99912 in posterior-scaled gradient space), while the dimensionless ratio ρ_f deletes the expansion scale exactly and responds primarily to Ω_m and w_a. Within flat w_0w_aCDM the family therefore adds interpretability rather than new constraining directions; whether the orthogonal complement grows in extended histories (early dark energy, non-CPL late-time evolution, or non-parametric $H(z)$ reconstructions, where age-like statistics are known to become more informative) is a natural follow-up question that the observable form of Section 3 is designed to make easy to answer.

Beyond diagnostics, the normalized clock connects to settings in which four-volume is itself the fundamental quantity: causal-set counting [4, 6] and unimodular time [7]. In those contexts $\mathcal{C}(T)$ is the natural dimensionless time variable of an FLRW universe, and its fraction boundaries are coordinate-free events. A companion paper develops the late-time limit: in an eternally accelerating future the causal four-volume remains unbounded despite the finite event horizon, and fixed increments $\Delta V_4 = f\,V_4(T_0)$ approach a finite, calculable proper-time spacing. We note in passing that the baseline value $T_{1/6} \simeq 8.65$ Gyr falls numerically close to long-count intervals that appear in traditional chronologies, a proximity remarked upon in popular accounts of cosmology [26].

What the construction enables. Beyond its individual results, the family unlocks capabilities that were not previously available in combination. First, it supplies a *calibration-independent referee* for the Hubble-tension debate: ρ_f is a scalar that distance-ladder-anchored and CMB-anchored analyses must agree on if flat w_0w_aCDM holds, because the disputed quantity H_0 is divided out exactly—disagreement in ρ_f cannot be attributed to the overall distance scale and must be located in (Ω_m, w_0, w_a). The referee role is scoped to flat FLRW with standard early-universe physics: sound-horizon assumptions, supernova calibration systematics, curvature, and neutrino physics still enter through the inferred shape of $H(z)$, so agreement in ρ_f localizes a disagreement rather than certifying either analysis. Second, the kernel of Section 7.1 converts the evolving-dark-energy question into a *node-contrast measurement* and tells surveys where the leverage lies: the negative lobe is fed by data below $z \simeq 0.40$ (DESI BGS, low-redshift supernovae, gravitational-wave standard sirens), the positive lobe by data at $z \simeq 0.5$–1.2 (DESI LRG and ELG tracers, the Euclid spectroscopic range), and the existing DESI tracer bins straddle the node almost symmetrically. Third, the kernel functions as a design tool: weighting data by $K_{f_*}(z)$ defines an estimator of w_a that is exactly H_0-free and first-order w_0-insensitive at the fiducial, with the second-order leakage bounded by Eq. (20); we present this as a construction for future work rather than a delivered result, since its noise properties depend on the survey. Finally, the same frozen normalization underlies the companion paper's future asymptotics: the present four-volume $V_4(T_0)$ that normalizes the clock also fixes the conditional 40.20 ± 1.6 Myr asymptotic increment spacing of an eternally Λ-dominated future. Together the pair tests the expansion history from both temporal directions—a past-facing diagnostic whose fingerprints discriminate ΛCDM from evolving dark energy in current chains, and a future-facing derived constant whose value labels the fate of the expansion—using one frozen formalism that others can apply, unchanged, to DESI DR3, Euclid, and standard-siren posteriors as they arrive.

Predictions. Three concrete, falsifiable statements follow from the frozen formalism. *(P1) A dimensionless null test.* Under flat ΛCDM the ratio statistic is fixed by the matter density alone: $\rho_{1/6} = 0.626682 \pm 0.000272$ for the Planck prior $\Omega_m = 0.3153 \pm 0.0073$. Evaluated at the DESI DR2 flat w_0w_aCDM central fits, the same statistic gives $\rho_{1/6} = 0.62529$, 0.62490, and 0.62507 (Pantheon+, Union3, DES-SN5YR)—displacements of 5–7 times the width of the ΛCDM *prior band* quoted above. The band-multiple figure quantifies calibration immunity, not detection significance: the definitive statistic is a two-posterior comparison transforming the ΛCDM and w_0w_aCDM chains through the same map, and, consistent with the 2.5–2.9σ displacement of $T_{1/6}$ in Table 2, that comparison yields a separation at approximately the 2.5–3σ level. Because ρ_f is exactly H_0-free, this separation cannot be absorbed by any recalibration of the distance ladder: forthcoming DESI and Euclid releases must either confirm the low value or restore the ΛCDM band, and Eqs. (6)–(7) are to be applied to those chains without modification. *(P2) The w_0-blind fraction.* At the ΛCDM-anchored point $f_* = 0.2627$, any CPL cosmology produces a computable offset of ρ_{f_*} that must, to first order, be attributable to (Ω_m, w_a) alone, with w_0 entering only through the quadratic leakage of Eq. (20); a measured displacement at f_* exceeding that quadratic bound yet requiring w_0 to explain would falsify the CPL description itself, and the migration of the node under alternative fiducials (Section 7.2) is part of the same signature. *(P3) Scaling of precision.* This is a local, fiducial-anchored forecast rather than a fundamental falsification test: the posterior width of $T_{1/6}$ contracts in fixed proportion to that of t_0 (alignment 0.99912), so the ± 16 Myr intervals of Table 2 are predicted to shrink with the age constraint of each future release; a violation of that proportionality would indicate a breakdown of the w_0w_aCDM parameterization.

Reproducibility. The reference implementation (quadratic-grid quadrature, the moment decomposition, and the chain-transformation scripts), together with the convergence tables of Appendix D, accompanies this paper.

A Derivation of the causal-past four-volume

The metric determinant of Eq. (2) is

$$g = -c^2 a^6(t)\, r^4 \sin^2\theta, \qquad \sqrt{-g} = c\, a^3(t)\, r^2 \sin\theta. \tag{25}$$

For a radial null ray, $\mathrm{d}s^2 = 0$ and $\mathrm{d}\Omega^2 = 0$, so

$$\mathrm{d}r = \frac{c\,\mathrm{d}t}{a(t)}. \tag{26}$$

Integrating Eq. (26) from an emission slice t to the endpoint T gives the comoving light-cone radius

$$\chi(t, T) = \int_t^T \frac{c\,\mathrm{d}u}{a(u)}. \tag{27}$$

The angular and radial integrations over the flat spatial slice are

$$\int \mathrm{d}\Omega = 4\pi, \qquad \int_0^\chi r^2\,\mathrm{d}r = \frac{\chi^3}{3}, \tag{28}$$

so the physical spatial volume of the slice is

$$V_3(t; T) = \frac{4\pi}{3}\, a^3(t)\, \chi^3(t, T). \tag{29}$$

The same result follows in Cartesian comoving coordinates by integrating $a^3(t)\,\mathrm{d}x\,\mathrm{d}y\,\mathrm{d}z$ over the ball $x^2 + y^2 + z^2 \le \chi^2$; spherical coordinates simplify the symmetry but are not a physical requirement.

The four-dimensional proper-volume element adds the factor $c\,\mathrm{d}t$,

$$\mathrm{d}V_4 = c\, V_3(t; T)\,\mathrm{d}t, \tag{30}$$

and integrating from the hot–big-bang limit to T yields

$$V_4(T) = \frac{4\pi c}{3} \int_0^T a^3(t) \left[\int_t^T \frac{c\,\mathrm{d}u}{a(u)} \right]^3 \mathrm{d}t, \tag{31}$$

which is Eq. (4) of the main text.

B Derivation of the redshift form

Change variables with

$$a = (1+z)^{-1}, \qquad \mathrm{d}t = -\frac{\mathrm{d}z}{(1+z)\,H(z)}. \tag{32}$$

The conformal radial interval between the endpoint redshift z_T and an emission redshift z becomes

$$\int_t^T \frac{\mathrm{d}u}{a(u)} = \int_{z_T}^z \frac{\mathrm{d}z'}{H(z')}, \tag{33}$$

and the volume measure transforms as

$$a^3\,\mathrm{d}t = -\frac{\mathrm{d}z}{(1+z)^4\,H(z)}. \tag{34}$$

Substitution of Eqs. (33)–(34) into Eq. (4) yields

$$V_4(z_T) = \frac{4\pi c^4}{3}\int_{z_T}^{\infty}\frac{\mathrm{d}z'}{(1+z')^4 H(z')}\left[\int_{z_T}^{z'}\frac{\mathrm{d}z''}{H(z'')}\right]^3. \tag{35}$$

Taking the ratio

$$\frac{V_4(z_f)}{V_4(0)} = f \tag{36}$$

cancels the prefactor $4\pi c^4/3$ and gives Eq. (7); the corresponding cosmic age is Eq. (6).

C Derivation of the self-similar limit

Let $a(t) = A\,t^p$ with $p < 1$. The comoving light-cone radius is

$$\int_t^T \frac{\mathrm{d}u}{A\,u^p} = \frac{T^{1-p} - t^{1-p}}{A\,(1-p)}. \tag{37}$$

Substituting Eq. (37) into Eq. (4) gives

$$V_4(T) = \frac{4\pi c^4}{3(1-p)^3}\int_0^T t^{3p}\left(T^{1-p} - t^{1-p}\right)^3 \mathrm{d}t. \tag{38}$$

With the rescaling $t = xT$, $\mathrm{d}t = T\,\mathrm{d}x$, the powers of T combine as

$$t^{3p}\left(T^{1-p} - t^{1-p}\right)^3 \mathrm{d}t = T^{\,3p+3(1-p)+1}\,x^{3p}\big(1 - x^{1-p}\big)^3\,\mathrm{d}x = T^4\,x^{3p}\big(1 - x^{1-p}\big)^3\,\mathrm{d}x, \tag{39}$$

so that

$$V_4(T) = \frac{4\pi c^4}{3(1-p)^3}\,T^4\int_0^1 x^{3p}\big(1 - x^{1-p}\big)^3\mathrm{d}x \equiv C(p)\,c^4\,T^4, \tag{40}$$

proving Eq. (8). The exponent 4 is independent of p: it counts one power of T from each spatial dimension of the light-cone slice and one from the proper-time accumulation.

D Numerical algorithm and convergence

For flat w_0w_aCDM define $E(a) = H(a)/H_0$ from Eq. (11). For an endpoint A, set $u_j = j/(N-1)$ and $a_j = A\,u_j^2$; the quadratic grid resolves the radiation-dominated limit without a finite early-time cutoff. The procedure is: (i) accumulate $t(a) = H_0^{-1}\int_0^a \mathrm{d}a'/[a'E(a')]$ and $\eta(a) = H_0^{-1}\int_0^a \mathrm{d}a'/[a'^2E(a')]$ with the analytic endpoint values $[a^2E(a)]^{-1}_{a=0} = \Omega_r^{-1/2}$ and $[aE(a)]^{-1}_{a=0} = 0$; (ii) accumulate the four moments of Eq. (22); (iii) form $V_4(a_j)$ from Eq. (23); (iv) locate the bracket of $V_4(a)/V_4(A) = f$ and interpolate a_f and $t(a_f)$ linearly across it, or, for maximal accuracy at a single fraction, solve $V_4(A_1)/V_4(1) - f = 0$ with Brent's method [25] at tolerances 2×10^{-11}. Unit conversion uses 1 Mpc $= 3.0856775814913673\times10^{19}$ km and 1 Gyr $= 365.25\times86400\times10^9$ s, i.e. 1 $\mathrm{Gyr}^{-1} = 977.79222\ \mathrm{km\,s^{-1}\,Mpc^{-1}}$.

Grid refinement for the baseline cosmology at $f = 1/6$:

Nodes N	$a_{1/6}$	$T_{1/6}$ (Gyr)	T_0 (Gyr)
2,001	0.670453614	8.645187823	13.795180940
4,001	0.670453935	8.645192833	13.795180964
8,001	0.670453988	8.645193619	13.795180970
16,001	0.670454015	8.645194048	13.795180972
32,001	0.670454015	8.645194039†	13.795180972

†All tabulated values use the moment decomposition of Section 8; the independent Brent-solved nested-quadrature implementation gives 8.645194042 Gyr at matching tolerances, in agreement to 3×10^{-9} Gyr. Doubling the grid from 16,001 to 32,001 nodes changes $T_{1/6}$ by 9 years.

E Chain transformation details

The posterior analysis uses the public DESI DR2 Cobaya products for flat w_0w_aCDM combining all DR2 BAO measurements with the baseline CMB likelihood (*Planck* 2018 low-ℓ TT and EE, NPIPE CamSpec high-ℓ TTTEEE, and *Planck*+ACT DR6 lensing) and one of Pantheon+, Union3, or DES-SN5YR [10]. All released text chains for each combination are read and verified against the released SHA-256 manifest. For each row the columns $(H_0, \Omega_m, w_0, w_a)$ are interpreted as in Eq. (11); spatial flatness and the released standard neutrino sector are retained, and Ω_r is recomputed per sample from $\Omega_r h^2 = 4.18343 \times 10^{-5}$. Each of the 100,918, 108,724, and 61,168 stored rows is evaluated once with its released multiplicity weight q_i; weighted quantiles use the midpoint cumulative-weight convention, with the central 68% interval given by the weighted 0.16 and 0.84 quantiles. For 128 fixed rows from each dataset, increasing the grid from 2,049 to 4,097 nodes changes $T_{1/6}$ by at most 7.8×10^{-6} Gyr; eighteen dispersed rows recomputed with the independent $N = 8001$ nested-quadrature implementation differ by at most 7.9×10^{-6} Gyr.

F Kernel computation: discretization and convergence

The sensitivity kernel of Section 7.1 is computed by finite localized perturbations about the ΛCDM baseline. The equation of state is set to $w(z') = -1 + \Delta w$ for $z' \in [z_{\rm lo}, z_{\rm hi}]$ and $w = -1$ outside, which multiplies the dark-energy density by

$$g(a) = \exp\left[3\,\Delta w\,\ln\frac{1 + \min\{\max(z, z_{\rm lo}), z_{\rm hi}\}}{1 + z_{\rm lo}}\right], \tag{41}$$

i.e. the perturbation accumulates only across the bin and rescales the density by a constant factor at all lower redshifts. The clock is evaluated on the quadratic scale-factor grid of Appendix D with $N = 8001$ nodes, and the kernel value assigned to the bin center is

$$K_f(z_c) = \frac{\rho_f[g] - \rho_f[1]}{\Delta w\,(z_{\rm hi} - z_{\rm lo})}, \tag{42}$$

with $\Delta w = 0.05$, bin width $\Delta z = 0.08$ for $z \le 1.6$ and $\Delta z = 0.2$ for $1.6 < z \le 3$; contributions beyond $z = 3$ are negligible at the plotted scale. Node locations are obtained by linear interpolation of the sign change. Convergence: halving both Δw and the bin width while doubling N moves the f_* node by less than 0.01 in redshift ($0.3953 \to 0.3945$), well below the quoted precision. The second-order leakage law, Eq. (20), is a quadratic fit to $\rho_{f_*}(w_0) - \rho_{f_*}(-1)$ evaluated on a uniform grid of nineteen constant-w_0 cosmologies spanning $w_0 \in [-1.30, -0.40]$.

References

[1] S. Park and R. P. Woodard, "The Volume of the Past Light-Cone and the Paneitz Operator," *Gen. Relativ. Gravit.* **42**, 2765–2783 (2010), https://doi.org/10.1007/s10714-010-1014-4.

[2] M. Carfora and F. Familiari, "Light cone comparison theorems and applications to relativistic cosmology," *Lett. Math. Phys.* **111**, 53 (2021).

[3] M. Carfora and F. Familiari, "How Dark is Dark Energy? A Lightcones Comparison Approach," *Gen. Relativ. Gravit.* (2025), https://doi.org/10.1007/s10714-025-03506-x.

[4] L. Bombelli, J. Lee, D. Meyer, and R. D. Sorkin, "Space-Time as a Causal Set," *Phys. Rev. Lett.* **59**, 521–524 (1987), https://doi.org/10.1103/PhysRevLett.59.521.

[5] R. D. Sorkin, "Forks in the Road, on the Way to Quantum Gravity," *Int. J. Theor. Phys.* **36**, 2759–2781 (1997), https://doi.org/10.1007/BF02435709.

[6] S. Surya, "The Causal Set Approach to Quantum Gravity," *Living Rev. Relativ.* **22**, 5 (2019), https://doi.org/10.1007/s41114-019-0023-1.

[7] M. Henneaux and C. Teitelboim, "The Cosmological Constant and General Covariance," *Phys. Lett. B* **222**, 195–199 (1989), https://doi.org/10.1016/0370-2693(89)91051-3.

[8] G. W. Gibbons and S. W. Hawking, "Cosmological Event Horizons, Thermodynamics, and Particle Creation," *Phys. Rev. D* **15**, 2738–2751 (1977), https://doi.org/10.1103/PhysRevD.15.2738.

[9] Planck Collaboration, N. Aghanim *et al.*, "Planck 2018 Results. VI. Cosmological Parameters," *Astron. Astrophys.* **641**, A6 (2020), https://doi.org/10.1051/0004-6361/201833910.

[10] DESI Collaboration, M. Abdul-Karim *et al.*, "DESI DR2 Results II: Measurements of Baryon Acoustic Oscillations and Cosmological Constraints," *Phys. Rev. D* **112**, 083515 (2025), https://doi.org/10.1103/tr6y-kpc6; official Cobaya chains, data model, and SHA-256 manifest, https://data.desi.lbl.gov/public/papers/y3/bao-cosmo-params/README.html.

[11] M. Chevallier and D. Polarski, "Accelerating Universes with Scaling Dark Matter," *Int. J. Mod. Phys. D* **10**, 213–224 (2001), https://doi.org/10.1142/S0218271801000822.

[12] E. V. Linder, "Exploring the Expansion History of the Universe," *Phys. Rev. Lett.* **90**, 091301 (2003), https://doi.org/10.1103/PhysRevLett.90.091301.

[13] D. Brout *et al.*, "The Pantheon+ Analysis: Cosmological Constraints," *Astrophys. J.* **938**, 110 (2022), https://doi.org/10.3847/1538-4357/ac8e04.

[14] D. Rubin *et al.*, "Union through UNITY: Cosmology with 2000 SNe Using a Unified Bayesian Framework," *Astrophys. J.* (2025), https://doi.org/10.3847/1538-4357/adc0a5.

[15] DES Collaboration, T. M. C. Abbott *et al.*, "The Dark Energy Survey: Cosmology Results with ∼1500 New High-Redshift Type Ia Supernovae Using the Full 5-Year Dataset," *Astrophys. J. Lett.* **973**, L14 (2024), https://doi.org/10.3847/2041-8213/ad6f9f.

[16] G. Efstathiou, "On DESI's DR2 Exclusion of ΛCDM," arXiv:2504.15336 (2025).

[17] H. Chaudhary *et al.*, "Implications of the DES-Dovekie Supernova Recalibration for Evolving Dark Energy," arXiv:2508.10514 (2025).

[18] "Bayesian Evidence for Dynamical Dark Energy After the DES-Dovekie Recalibration," arXiv:2511.10631 (2025).

[19] D. Huterer and M. S. Turner, "Probing Dark Energy: Methods and Strategies," *Phys. Rev. D* **64**, 123527 (2001), https://doi.org/10.1103/PhysRevD.64.123527.

[20] A. Albrecht *et al.*, "Report of the Dark Energy Task Force," arXiv:astro-ph/0609591 (2006).

[21] T. D. Saini, T. Padmanabhan, and S. L. Bridle, "Response of Distance Measures to the Equation of State," *Mon. Not. R. Astron. Soc.* **343**, 533 (2003).

[22] S. Lee, "Structural Limitations on Constraining the Time Evolution of Dark Energy: An Exact Linear Response Approach," *Phys. Lett. B* **874**, 140237 (2026), arXiv:2512.14747.

[23] L. Kazantzidis, L. Perivolaropoulos, and F. Skara, "Constraining Power of Cosmological Observables: Blind Redshift Spots and Optimal Ranges," *Phys. Rev. D* **99**, 063537 (2019), https://doi.org/10.1103/PhysRevD.99.063537.

[24] D. Huterer and G. Starkman, "Parameterization of Dark-Energy Properties: A Principal-Component Approach," *Phys. Rev. Lett.* **90**, 031301 (2003), https://doi.org/10.1103/PhysRevLett.90.031301.

[25] R. P. Brent, *Algorithms for Minimization without Derivatives*, Prentice-Hall (1973), Chapter 4.

[26] C. Sagan, *Cosmos*, Random House (1980), Chapter 10.